IEEE Access
Multidisciplinary | Rapid Review | Open Access Journal

Received February 28, 2020, accepted March 23, 2020, date of publication April 27, 2020, date of current version May 12, 2020.

*Digital Object Identifier 10.1109/ACCESS.2020.2990403*

# Imaging Conductive Objects Through Metal Enclosures Using ELF/VLF Magnetic Fields

**HO Y. KIM[1], (Member, IEEE), VIJAY HARID[1], (Member, IEEE), ALEXANDER MROZ[1], JOSHUA WEWERKA[1], DALIBOR J. TODOROVSKI[1], MARK GOŁKOWSKI[1], (Member, IEEE), RONALD A. L. RORRER[2], (Member, IEEE), MORRIS B. COHEN[3], (Senior Member, IEEE), AND NATHAN M. OPALINSKI[3]**

[1]Department of Electrical Engineering, University of Colorado at Denver, Denver, CO 80204, USA
[2]Department of Mechanical Engineering, University of Colorado at Denver, Denver, CO 80204, USA
[3]Department of Electrical and Computer Engineering, Georgia Institute of Technology, Atlanta, GA 30332, USA

Corresponding author: Ho Y. Kim (hoyoung.kim@ucdenver.edu)

This work was supported by the Defense Advanced Research Projects Agency (DARPA)-Imaging Through Almost Anything Anywhere (ITA3) program under Contact HR00111820016.

**ABSTRACT** Imaging through conductive media is a pervasive problem in medical, industrial, and security applications. Several potential modalities such as X-ray, exotic particle beams, and related high resolution techniques have been employed in the past. However, the difficulty of production and safety of these technologies is a concern in practice. Of particular interest in this work are extremely and very low frequency (ELF/VLF, f<30 kHz) radio signals. We consider the feasibility of using ELF/VLF signals for detecting and imaging objects that are hidden inside thin-shelled conductive enclosures. It is shown that the hidden perfect electrical conductor (PEC) object partially blocks the incident magnetic field and results in a magnetic-field depletion that can be used to detect the object. Next, using FEKO simulations, a parametric study of through-conductor detection using a magnetic dipole is considered for a cubic aluminum shield. It is shown that signals above 1 kHz can be used to evaluate the outer shield properties, while signals at frequencies below 200 Hz can be used to effectively discern shapes of hidden objects by observing the magnetic distortion within 1 cm of the outer shield. To validate the results of theory and simulations, experiments matching the simulation conditions are conducted with a cubic aluminum container and hidden aluminum block. The experiments clearly demonstrate the presence of the magnetic field depletion as predicted by theory and simulations. The results of this work suggest that near-field ELF/VLF magnetic induction is an effective method for imaging through realistic metallic shields.

**INDEX TERMS** Computational electromagnetics, extremely low frequency, near-field, nondestructive evaluation, surface integral equation, through conductor imaging, very low frequency.

## I. INTRODUCTION

ELF/VLF signals (f<30 kHz) have been widely used over several decades for radio waves, geophysical prospecting, submarine communications, and upper atmospheric remote sensing [1]–[5]. Background ELF/VLF signals have been also employed for passive imaging applications due to the global presence of power line radiation, Navy transmitter signals, background lightning radiation (sferics), and cosmic sources [5]. The primary reason is that ELF/VLF signals can penetrate conductive barriers (ground, seawater, metal shields, etc.) that are otherwise inaccessible for higher frequency radiation [6]. In this work, we investigate the utility of ELF/VLF signals for detecting metal objects that are obscured by highly conductive shields. The motivation is to investigate the possibility of imaging through highly conductive media using ELF/VLF magnetic induction tomography (MIT) [7] or similar methods. From a practical point of view, the analysis is relevant for non-destructive evaluation of conductive objects inside metal containers for industrial and security applications.

MIT has recently garnered considerable attention as a novel method for non-destructive evaluation (NDE) in industrial and medical applications [8]–[10]. The typical methodology for inspecting conductive structures surrounds the target of interest with an array of several inductive coils. One of

The associate editor coordinating the review of this manuscript and approving it for publication was Su Yan.

the coils is excited at frequencies in the range of 5-500 kHz [11] while the remaining coils are treated as receivers. Based on the receiver measurements, image reconstruction can be performed via appropriate inversion algorithms [12], [13]. MIT has proven to be quite successful for inspecting metallic structures for deformities when the surrounding medium is air or mildly conductive media such as saline ($\sigma \approx 1\frac{S}{m}$) [7]. Although commonly used MIT frequencies contain the ELF/VLF band, previous work has not considered inspection of metallic objects that are surrounded by a highly conductive shield ($10^5\frac{S}{m} < \sigma < 10^8\frac{S}{m}$). As such, the primary objective of this work is to consider the efficacy of ELF/VLF magnetic fields for the detection of shielded metallic objects.

Section II considers analytical expressions and approximations for a spherical perfect electrical conductor (PEC) on the internal surface of a conductive shell when illuminated by a low frequency magnetic field. In particular, it is shown that the hidden PEC object results in a magnetic-field depletion region that carries information about the object. Section III utilizes FEKO simulations to parametrically evaluate the impact of frequency, measurement distance, and object shape on ELF/VLF through-shield imaging. Section IV then discusses experimental results with a aluminum block that is placed on the internal surface of a aluminum container. It is shown that the experimental results clearly display the magnetic-field depletion that is consistent with theory and simulations. Section V provides a summary of the results with implications for future work.

## II. NEAR-FIELD MAGNETIC DISTORTION THEORY

Modeling near-field scattering of ELF/VLF signals by shielded objects is analytically tractable for only a few selected geometries. However, the general principles can be understood by analyzing magnetic field distortions due to spherical objects and thin-shelled spherical shields. Specifically, we consider the problem of a thin spherical shield of outer radius $a$, shield thickness $d$ and conductivity $\sigma$. The center of the spherical shield is located at the origin. A spherical PEC object of radius $R$ is assumed to be inside the shield with its center located at $r_0$ as shown in Fig. 1. The source is assumed to be a uniform z-directed magnetic field phasor $H_0 = H_0\hat{z}$ with angular frequency $\omega$. Additionally, the fields are assumed to be measured on a plane at a distance $\delta r$ that is displaced along the direction that is normal to the external sphere and along the incident magnetic field direction. To examine the relative effects of the shield and the PEC object, the total magnetic field is decomposed into $H = H_S + H_P$. Here, $H_S$ corresponds to the total magnetic field in the presence of an empty spherical shield. The quantity $H_P$ includes the additional distortion to the magnetic field due to the hidden PEC sphere.

Determining a closed form expression for $H_S$ in the near-field limit is fruitful for the present analysis. The general abstract problem of scattering of electromagnetic plane waves by concentric spherical shells of arbitrary material properties has been studied by numerous authors for more than a century [14], [15]. However, the analysis can be considerably simplified in the long-wave limit for $a \ll \lambda$ where $\lambda$ represents the free-space wavelength. It is worth noting that plane-wave analysis is justified since it is effectively equivalent to a homogeneous magnetic field in the low frequency limit where $\frac{a}{\lambda} \ll 1$. Specifically, it can be shown that in the free-space region inside the spherical shell, $0 \le r < a - d$, the magnetic field is given by,

$$H_S = SE_H^{-1} H_0 \tag{1}$$

The quantity $SE_H$ is the magnetic shielding effectiveness with a closed form expression given by [14],

$$SE_H = \cosh(kd) + \frac{1}{3}\left(ka + \frac{1}{ka}\right)\sinh(kd) \tag{2}$$

In contrast, the magnetic field in the free-space exterior region, $r > a$ is the sum of the incident field and that of an ideal magnetic dipole centered at the origin with magnetic moment, $m_S$. The magnetic dipole moment is given by [16],

$$m_S = -2\pi a^3 A H_0, \tag{3}$$

where the quantity $A = \left[\frac{j\omega\sigma\mu_0 ad}{j\omega\sigma\mu_0 ad+3}\right]$.

It can be seen that for high conductivity shields $\sigma \to \infty$, the quantity $A \to 1$ and reverts to the well-known solution of a PEC sphere immersed in a uniform magnetic field [16]. The critical importance of frequency $\omega$ is apparent since sufficiently low frequencies offset high conductivities and can be used to more easily penetrate the thin shield and detect hidden metal objects. Thus, examining the frequency dependence of the distorted magnetic field is a useful method for separating the shield from potential hidden objects [17].

In principle the quantity $H_P$ can be determined exactly by representing the solution via an infinite summation expansion of vector spherical harmonics [18]. However, the general expression for a non-concentric PEC sphere is sufficiently complicated that useful abstract features can be overlooked. As such, we thus invoke heuristic approximations to more easily include the effect of the hidden PEC sphere.

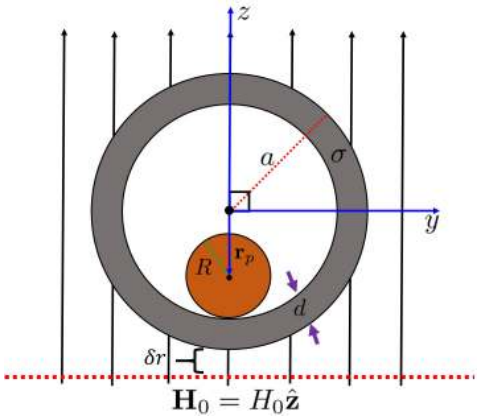


**FIGURE 1.** Geometry for PEC sphere shielded by a spherical conductive object in a z-directed uniform magnetic field. $H_0$ is the magnetic field in the absence of the shield.

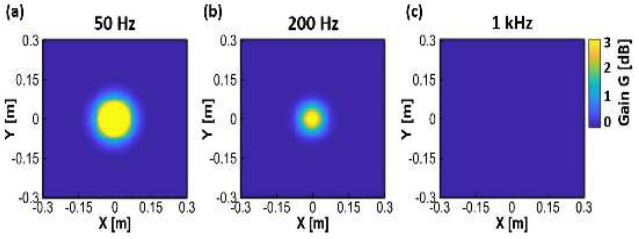


**FIGURE 2.** Magnetic gain *G* function at (a) 50 Hz, (b) 200 Hz and (c) 1 kHz corresponding to a PEC sphere inside a spherical thin-shell shield.

In the interior of the shield, the magnetic field $H_S$ is assumed to be approximately uniform, which is well justified by previous work [16]. Additionally, the multiple reflections between the internal shield walls and the PEC object are also neglected which is similar to the Born approximation. In invoking these approximations, the solution to the problem of a PEC sphere immersed in a uniform magnetic field, $H_S$, can be utilized. The magnetic field will induce surface currents on the PEC sphere that can be equivalently modeled as an induced magnetic dipole $m_P$,

$$m_P = -\frac{2\pi R^3}{SE_H} H_0 \tag{4}$$

The total field $H$ at the receiver is thus approximated as the superposition of the fields from the dipole $m_S$, the dipole $m_P$, and the incident field $H_0$. Assuming the impact of an empty box or shell can be calibrated (which is a reasonable assumption for several inspection applications), the gain $G$ can be defined as $G = \frac{|H_S \cdot \hat{z}|}{|H|}$ which is the ratio of the field in the absence of the hidden object to the normal component of the field with the object present.

The gain $G$ for the z-component (same as primary field component) of the magnetic field is shown in Fig. 2 for a=0.74 m, d=2.7 mm, R=.1 m, $\sigma$=3.53×10$^7$ $\frac{S}{m}$, $r_p$=(0,0,−0.6417 m). The measurement plane is located at $r$=(x,y,−0.7494 m). The aforementioned parameters are selected in accordance with the experimental setup that is presented in Section IV. As shown in Fig. 2, the gain shows a deviation from the empty shield case. Specifically, a magnetic-field depletion (or equivalently enhancement of the gain, $G$) is clearly visible at 50 Hz and to a less extent at 200 Hz. At 1 kHz, $A \approx 1$ and the outer shield itself acts effectively like a PEC sphere and completely blocks the hidden PEC object which shows the utility of the lower frequency signals for penetrating a conductor. The presence of the increased gain at lower frequencies is simply because the induced magnetic dipole moment shown in 4 is anti-parallel to the shielded magnetic field $H_S$. Thus, the additional fields due to the PEC object will be anti-parallel to the incident field when measured along the axis of the induced dipole moment. Since the frequencies required to penetrate conductors are in the ELF/VLF band, the wavelengths are always in the kilometer range. As such, the physics of the problem is always in the quasi-static (or near-field) regime and every object can be considered electrically small. Thus, the frequency dependence primarily enters as the skin-depth phenomena (for penetration) but is not strongly related to object size. There is a dependence of frequency on geometry when finite conductivity/permeability objects are considered. However, in the limit of PEC objects, frequency does not show up in the equations at all. This key feature can thus be leveraged for detecting highly conductive objects that are otherwise obscured by thin-shell shield.

The previous analysis is quite approximate and is primarily meant to present the useful feature of the magnetic field depletion. A more general and accurate analysis is analytically intractable and as such a numerical approach is more appropriate. In the following section, numerical simulations are used to sweep over relevant parameters and examine important aspects of near-field magnetic distortions for non-destructive evaluation through conductive shields.

## III. SIMULATION STUDY

The primary focus of the simulation study is to evaluate the efficacy of detecting PEC objects inside a aluminum container using a transmitting loop antenna. The parameters used in the numerical study are consistent with that of performed experiments described in Section IV. The simulations employ the commercial electromagnetic software, FEKO [19], which utilizes a hybrid frequency-domain finite element and boundary element solver. We employ the frequency domain method of moments (MoM) using the surface integral equation (SIE) option in FEKO. This method is well-suited to shielding problems since the surface area to volume ratio is low. The shielding container is only 2.7 mm in thickness, however, the skin depth can be just a fraction of a millimeter at 1 kHz. Using methods like finite difference time domain (FDTD) or finite element method (FEM) would force a large number of simulation cells to resolve the skin depth inside the material. Furthermore, the air-region inside the container will also need to be meshed using FDTD/FEM. This air-region occupies 98.7% of the total volume of the container and will require a large number of cells using FDTD/FEM. The MoM-SIE formalism only meshes the surfaces of the container and the hidden objects while the air region is implicitly included in the Green's functions. Thus the MoM approach allows at least an order of magnitude less of simulation cells (and computation time) compared to FDTD/FEM.

### A. BASIC SIMULATION RESULTS

It is useful to first expand on the analytical estimates from Section II using simulations. In this manner, the qualitative description of the magnetic-field depletion can be verified without needing approximations. Fig. 3 shows a simple simulation result of a PEC cylinder in the presence of a point magnetic dipole (proxy for loop antenna). Specifically, the cylinder has radius and height that are both 0.2 m. The transmitting magnetic dipole is negative $z$-oriented with amplitude 1 A·m$^2$. The dipole is elevated 0.2 m above the central axis of the cylinder PEC and transmits at 50 Hz. The

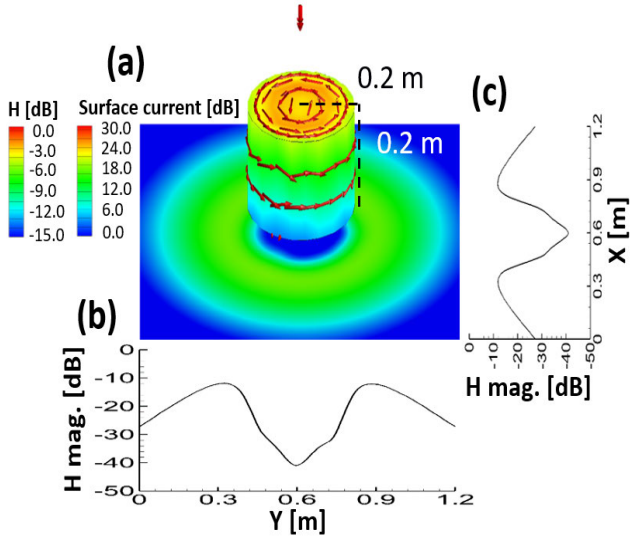


**FIGURE 3.** The magnetic field and surface current of PEC in near-field of a loop antenna. For PEC in a cylinder geometry, the radius and height are 0.2 m. (a) H magnitude at Z=−0.05 m, (b) H magnitude along *y*-direction at X=0.6 m, and (c) H magnitude along *x*-direction at Y=0.6 m.

red arrows on the surface of the cylinder, shown in Fig. 3(a), represent the induced surface currents. The surface currents are induced to satisfy the boundary condition of zero normal magnetic field on the surface. The currents are thus forced to flow in the counterclockwise direction such that the induced field opposes the incident field on the surface of the PEC. The counterclockwise loops of surface current can be abstracted as a *z*-oriented magnetic dipole. The induced dipole moment is thus anti-parallel to the transmitting dipole. Thus, along the axis of the source and cylinder, the induced dipole will generate a magnetic field that opposes the incident field and will result in a magnetic field deletion. The magnetic field depletion is readily observed in Fig. 3(a) on a plane located 0.05 m below the base of the cylinder. Fig. 3(b) and Fig. 3(c) show the H-field magnitudes at Z=−0.05 m along the *y*-direction (X=0.6 m) and along the *x*-direction (Y=0.6 m) respectively. Specifically, the field magnitude is observed to decrease approximately 30 dB in the region directly below the cylinder. The relatively large change in the field magnitude motivates investigating ELF object detection with the addition of a conductive shield.

The simulations are further extended to include the presence of a metallic shield. Fig. 4 shows the simulation setup of a PEC cube inside a aluminum box shield. The aluminum box has a conductivity of $1 \times 10^7$ S/m with side length L=1.2 m and thickness d=2.7 mm. The hidden PEC has length 0.2 m with the center of the PEC base located at Z=d, and X=Y=L/2. The transmitter is a negative *z*-oriented magnetic dipole located at Z=1.21 m, and X=Y=L/2 with a dipole-moment of 1 $Am^2$. The locations of the transmitter, aluminum box, and PEC are fixed as shown in Fig. 4. The simulations utilize 8,770 surface elements with 1 cm grid length of field points.

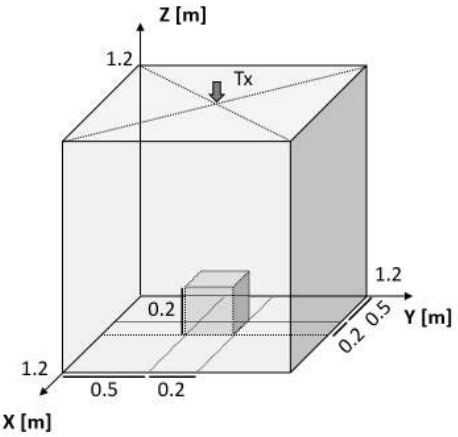


**FIGURE 4.** Illustration of simulation setup of a PEC cube inside a aluminum box shield in near-field of a loop antenna. The aluminum box is a conductive shell in a cubic geometry. The thickness is 2.7 mm and the conductivity is $1 \times 10^7$ S/m.

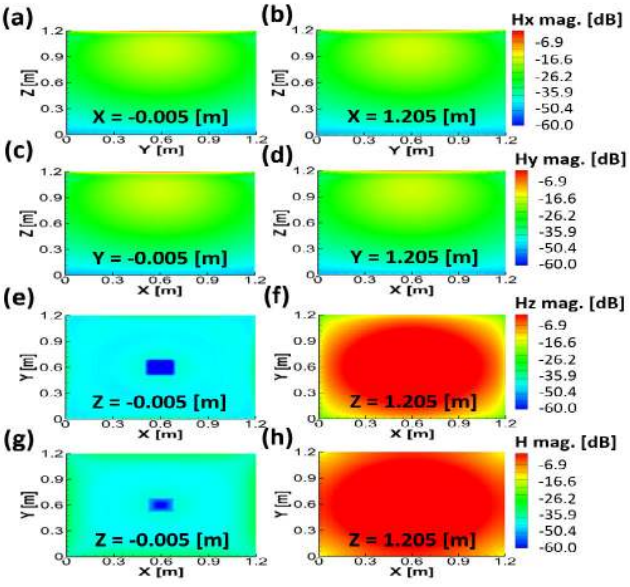


**FIGURE 5.** Measurement of normal components on each face. Hx magnitude at (a) X=−0.005 and (b) 1.205 m on yz-plane. Hy magnitude at (c) Y=−0.005 and (d) 1.205 m on xz-plane. Hz and H magnitudes at (e, g) Z=−0.005 and (f, h) 1.205 m on xy-plane.

Fig. 5(a)-(f) show the normal components of the magnetic field relative to the six faces of the box for a source frequency of 50 Hz. The normal components are measured at a 0.005 m distance from the surface of each face.

As shown in Fig. 5(e), the magnetic field amplitude behind the hidden PEC cube is reduced by approximately 20 dB compared to surrounding field. The region of magnetic field depletion approximately outlines the hidden PEC object. This suggests that hidden objects can not only be detected but geometrical features can also be readily discerned. As shown in Fig. 5(g) and (h) show the H-field magnitude is approximately the same as the normal field components shown in

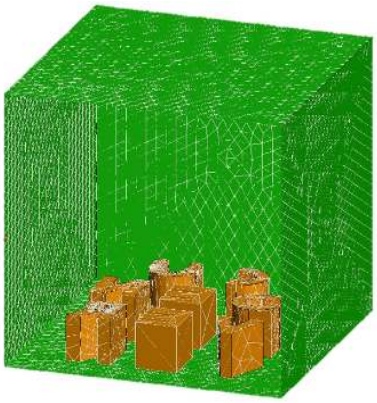

**FIGURE 6.** Simulation setup of eight PEC objects inside a aluminum box shield.

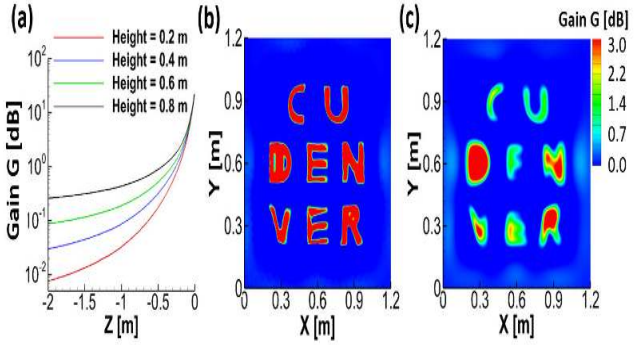


**FIGURE 7.** Measurement of the gain *G* on one magnetic dipole for different (a) heights of the inside box. Distinguishing multiple object shapes (PEC) with a single plain wave with *z*-directed B-field at (b) Z=−0.005 m and (c) −0.04 m on xy-plain.

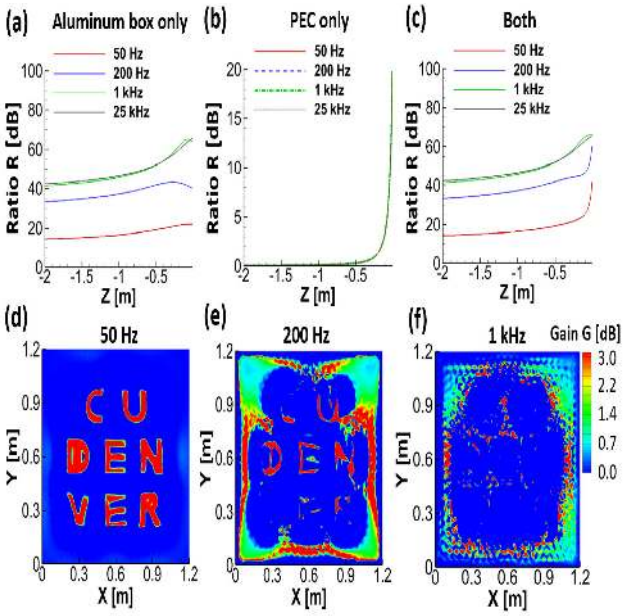


**FIGURE 8.** The magnitude ratio *R* for different frequencies for (a) only aluminum shield ($\sigma = 1 \times 10^7$ *S/m*, $\epsilon_r = 1$), (b) only PEC, (c) aluminum shield with hidden PEC object. The gain *G* measured at Z=−0.005 m (d) 50 Hz, (e) 200 Hz, and (f) 1 kHz.

panel (e) and (f). This further justifies measuring only the normal component of the fields for the purpose of imaging. Although this is a trivial simplification from a simulation point of view, measuring only the normal component greatly simplifies experiments (as seen in Section IV).

### *B. PARAMETRIC STUDY*

The previous simulations have shown the utility of using ELF signals for imaging hidden PEC objects inside a metallic shield. Next, the simulations are extended in a parametric manner to examine the effect of object shape and size, measurement plane distance, and frequency.

The same aluminum container used in previous simulations is filled with eight PEC objects as shown in Fig. 6. The objects are shaped in a manner to spell out ''C-U-D-E-N-V-E-R'' which provides some diversity in the object shapes and locations.

Fig. 7(a) shows *G* along the central *z*-axis of the aluminum shield starting from the base (Z=0) and extending below by 2 m. Each curve corresponds to different heights of the PEC objects while keeping the X and Y dimensions fixed. At Z=0, *G* decreases from 22.2 dB to 21.2 dB when the height of the PEC increases from 0.2 m to 0.8 m. At Z=−0.5 m, the difference between height 0.2 m and 0.8 m is 0.7 dB and it decreases at a farther distance away from the aluminum shield. This demonstrates that the taller the hidden object, the further the magnetic depletion extends in the direction normal to the shield surface. That is, the height of the hidden object can be discerned by measuring the H-field at incrementally greater distances from the shield surface. At the same time, the transverse geometries of the hidden objects are very clearly delineated. This is shown in Fig. 7(b) and (c) where the measurement planes are at Z=−0.005 m and Z=−0.04 m respectively.

As shown, the measurement at Z=−0.005 m and Z=−0.04 m shows the object shapes quite clearly. However, the dynamic range is approximately 10 dB lower when the measurement plane moves from Z=−0.005 m to Z=−0.04 m as shown in Fig. 7(a). This is expected since the fields fall off as $\frac{1}{D^3}$ where $D$ is the distance from the object. Thus greater measurement distance will make the field distortions decrease while ''blurring'' the object shapes to an extent. In regards to practical scenarios, 0.04 m is still a reasonable standoff distance for taking measurements with small magnetic coil receivers, this is demonstrated with experiments in Section IV. To extend the measurement distances, the experiment would need to be moved to a less cluttered environment and the incident signal to noise ratio (SNR) should also be increased. The primary takeaway from Fig. 7(b) and (c) is that hidden objects on the surface of metallic shields can in fact be detected and imaged even without complex inversion techniques.

The simulation results are then further extended to investigate the dependence of object detection on transmit frequency. Fig. 8 shows the relative impact of frequency along

with standoff distance. Panels (a)-(c) show the magnitude ratio $R$ of the incident magnetic field $H_0$ to the total magnetic field $H$ ($R = \frac{|H_0|}{|H|}$) along the $z$-direction starting 2 m below the box up to the base at Z=−0.005 m. The ratio $R$ is measured along the $z$-line that intersects the center of the box at X=Y=0.6 m. Specifically, panel (a) shows the field ratio due to an empty aluminum box. This serves as a calibration and also demonstrates the relative frequency effect with the outer shell alone. As shown at 50 Hz, the value of $H$ is relatively compared to other frequencies. As discussed in Section II, this is because the 50 Hz signal is relatively transparent to the incident signal which results in a small induced dipole moment on the aluminum shell. As the frequency is increased to 1 kHz the aluminum shell begins to resemble a PEC box. As shown, the 1 kHz and 25 kHz cases results show approximately the same field ratio since the box is effectively a PEC at these frequencies. This suggests that frequencies below ≈1 kHz are more useful to penetrate the 2.7 mm aluminum shield to an appreciable extent. Fig. 8(b) shows the field ratio with an isolated PEC. As discussed in Section II, the magnetic moment induced on a PEC sphere is independent of frequency in the long-wave limit. As such, the field ratio is the same for all frequencies as expected. Fig. 8(c) shows the result of the full problem of a hidden PEC object inside the aluminum shield. As shown in Fig. 8(a), for 1 kHz and 25 kHz the result is the same as the empty aluminum shield shown. Again, this is because the outer shield effectively blocks the incident field and does not permit detection of the hidden object. On the other hand, the 50 Hz and 200 Hz cases both differ from the empty shield case at positions close to the base of the shield Z≈−0.005 m. At distances approaching Z=2 m the empty box case (a) and hidden object case (b) once again approach the same answer. This is for the same reason as Fig. 7(b)-(c) where the field distortion due to the hidden objects become less prominent with increasing standoff distance. The impact of frequency is further illustrated in Fig. 8(d)-(f) where the gain $G$ is measured at Z=−0.005 m for three frequencies. As the frequency is progressed from 50 Hz to 1 kHz, the hidden objects become less prominent as the aluminum box becomes a more effective shield.

It is worth noting that all the simulations consider PEC hidden objects. In practice, the finite conductivity of materials can have an additional important impact on the frequency dependence. As such, the basic idea of scanning the normal component of the field at the surface of the shield along with sweeping frequency remains a valid experimental principle. Experimental results that closely correspond to the simulation parameters are discussed in Section IV.

## IV. EXPERIMENTAL VALIDATION

To validate the results of simulations, an experiment with an aluminum container with an aluminum block placed inside was conducted. The experiment was conducted indoors on the University of Colorado Denver campus with considerable environmental clutter (metal fixtures, wiring, etc.) and large amounts of radio noise. The environment was selected to demonstrate the robustness of ELF/VLF through conductor imaging in a realistic environment.

**FIGURE 9.** Photograph of the transmitting loop source fastened to the external face of the container.

The cubic container has side lengths of 1.2 m and wall thickness of 2.7 mm, as consistent with the FEKO simulations. The container has 5 welded sides and a single removable face that can be bolted on. For the source, a 0.5 m radius loop antenna consisting of 10 turns of 12 gauge copper wire was fastened to the opposite side of the box relative to the object. The loop antenna is a more realistic proxy of the magnetic dipole used in the simulations described in Section III. Since the frequencies considered in this experiments are within the audible acoustic spectrum, the transmitting loop was driven by an audio amplifier (Planet Audio AC1200.2 Anarchy 1200 Watt, 2 Channel, 2/4 Ohm Stable Class A/B, Full Range). A photograph of the transmit loop on the container (bolted faced removed) is shown in Fig. 9. The rectangular aluminum block was placed on the inner face of the container and is 6.5 cm thick, 16 cm wide, and 23.5 cm long. The long edge was positioned vertically relative to the ground with the base elevated 30 cm from the bottom of the container using a wooden stand. The center of the block was placed 60 cm from either side of the container. This placement was to ensure that the face with the largest surface area was coplanar with the face of the shield. A photograph of the hidden aluminum object inside the container is shown in Fig. 10.

As demonstrated in Section III, the magnetic field normal to the container's exterior can have extremely fine spatial resolution, however, the resolution fades rapidly with measurement distance from the surface of the container. To match the results of the simulations, a high resolution grid of point magnetic field measurements are required on the exterior face that is coplanar with the hidden object. As such, a 10 x 10 grid of measurement points with a 5 cm grid spacing was ensured using a fastened pegboard and attached dowels to place the receiver. The total area of the grid covers 70 cm x 70 cm around the hidden object. The receiver is a 10 cm square loop antenna that utilizes a sophisticated design based

**FIGURE 10.** Photograph of the rectangular aluminum block on the internal face of the container.

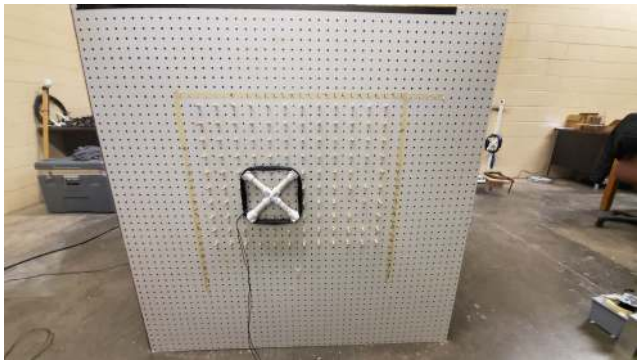

**FIGURE 11.** Photograph of the receiver array to scan for the hidden aluminum object.

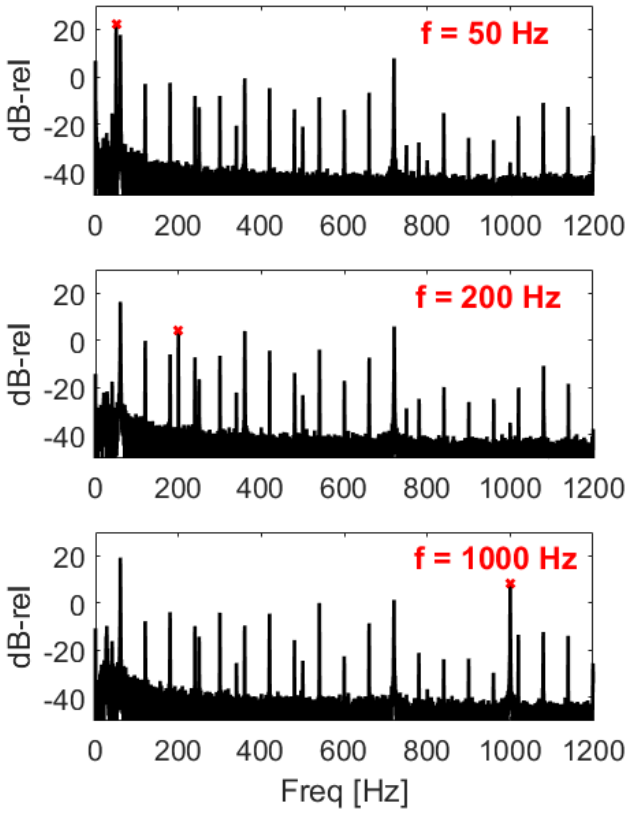


**FIGURE 12.** Example frequency spectra for 50 Hz, 200 Hz, and 1 kHz in the empty aluminum box condition.

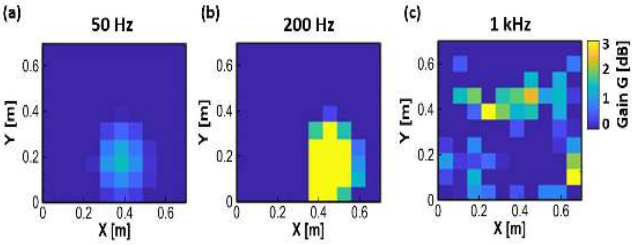


**FIGURE 13.** Results from experiment with hidden object inside the surface of an aluminum container with (a) 50 Hz, (b) 200 Hz, and (c) 1 kHz.

on specifications described in [20]. The 10 cm width of the receiving loop ensures fifty percent overlap between adjacent positions. Each measurement lasts sixty seconds. Thus, one scan of the face takes approximately 100 minutes per transmit frequency. The experiment is repeated with and without the object and thus takes 200 minutes for one experimental result. A photograph of the loop antenna along with the pegboard array is shown in Fig. 11.

The loop transmitter was run at three frequencies: 50 Hz, 200 Hz, and 1 kHz. These frequencies were selected to demonstrate the frequency dependence of detection as well as to not overlap with power-line harmonics. Samples received spectra for each transmit frequency (60 second integration) in the presence of the empty box are shown in Fig. 12. The 50 Hz signal (marked by red x in the top panel) is shown to be approximately 60 dB above the noise floor which is expected to be sufficient based on simulation results. The 200 Hz and 1 kHz signals are approximately 40 dB and 50 dB above the noise floor respectively and are also expected to have a sufficiently high SNR for object detection. The unlabeled spikes on the spectra correspond to power-line harmonics as well as fields from unknown electronic sources. The 20-30 dB of SNR even in the presence of significant interference suggests that the full 60 second integration times were not needed and can be reduced in the future.

Fig. 13 shows measured values of the magnetic field deviations at 50 Hz, 200 Hz, and 1 kHz. All the results are relative to the baseline empty container case. As shown, the hidden aluminum object is clearly visible as a magnetic field depletion in the 50 Hz and 200 Hz cases. At 1 kHz, the object cannot be detected because the magnetic field can not appreciably penetrate the container. The noise-like variations at 1 kHz occur because the two way penetration through the container results in approximately 80 dB of loss [21], which is below the background noise floor. The results are consistent with simulations in Section III and provide good justification for using ELF/VLF signals as part of through conductor detection applications.

The experiments show certain important features that deviate from the simulation results and warrant further discussion. One such deviation is that the 50 Hz experiment scenario shows a dimmer outline of the object in comparison to the

200 Hz case. This is likely due to the fact that the simulations focused on PEC objects while the experiments utilized an aluminum object. Although the penetration into the container is highest in the 50 Hz case, the aluminum object scatters less than a PEC since there is appreciable penetration into the object itself (1.2 cm skin depth at 50 Hz). Varying material properties of the hidden object was not explored in the simulations, however, the experimental results suggest a clear frequency dependence. Specifically, the induced dipole moment on a finite conductivity object is well-known to have a strong dependence on frequency in the ELF/VLF range [18], [22]. A second deviation is that the measurements are not at points but rather integrated measurements over the area of the 10 cm x 10 cm receiving loop. Thus, the location with the object is likely undersampled which leads to a blurring of the constructed image.

The experimental results show that nondestructive evaluation for the size, position, and material properties of a hidden object inside a realistic container is possible using ELF/VLF magnetic fields. The investigations in this works have primarily considered a hidden aluminum object inside an aluminum container. Additionally, the object was directly adjacent to an internal face of the shield. Under these constraints, theoretical and experimental investigation has shown that the hidden object is easily detectable without complex image reconstruction methods. However, as the location of the object and geometric complexity is varied, more sophisticated methods of image reconstruction would be required. Such methods have been heavily studied in static and quasi-static reconstruction technologies such as electrical capacitance tomography (ECT), electrical impedance tomography (EIT), MIT [23]. Thus, the methodology employed in this work can be directly extending for more complex scenarios. Topics for ongoing work includes varying object material properties, developing automated scanning for higher resolution measurements, and employing quasi-static inversion algorithms for tomographic image reconstruction.

## V. CONCLUSION

ELF/VLF imaging and nondestructive evaluation of conductive objects hidden inside a metal container is investigated with theory, simulations, and experiment. Analytical approximation show that PEC objects inside a thin-shelled metal container results in a magnetic field depletion at the exterior of the container. The depletion is primarily observed for the normal component of the field in relation to the shield surface. Using simulations, a parametric study is to evaluate the importance of standoff distance, frequency, and object size. It is shown that hidden objects on the interior surface of an aluminum shield can be robustly detected for frequencies below 200 Hz for standoff distances less than 5 cm. An experiment of a hidden aluminum object inside an aluminum container is conducted using an ELF/VLF loop antenna. The experiment clearly demonstrated the magnetic depletion effect and shows good agreement with simulation results. The results of the work justify the use of ELF/VLF magnetic induction fields for non-destructive evaluation through highly conductive enclosures.

## REFERENCES

[1] S. A. Cummer, U. S. Inan, and T. F. Bell, "Ionospheric D region remote sensing using VLF radio atmospherics," *Radio Sci.*, vol. 33, no. 6, pp. 1781–1792, Nov. 1998.
[2] J. R. Wait, "Theory of magnetotelluric fields," *J. Res. Nat. Bur. Standards, D, Radio Propag.*, vol. 66, no. 5, pp. 509–541, Sep. 1962.
[3] L. B. Pedersen and M. Engels, "Routine 2D inversion of magnetotelluric data using the determinant of the impedance tensor," *Geophysics*, vol. 70, no. 2, pp. G33–G41, Mar. 2005.
[4] P. Hosseini, M. Gołkowski, and V. Harid, "Remote sensing of radiation belt energetic electrons using lightning triggered upper band chorus," *Geophys. Res. Lett.*, vol. 46, no. 1, pp. 37–47, Jan. 2019.
[5] M. Gołkowski, S. R. Sarker, C. Renick, R. C. Moore, M. B. Cohen, A. Kułak, J. Młynarczyk, and J. Kubisz, "Ionospheric D region remote sensing using ELF sferic group velocity," *Geophys. Res. Lett.*, vol. 45, no. 23, pp. 12,739–12,748, Dec. 2018.
[6] J. D. McNeill and V. F. Labson, "Geological mapping using VLF radio fields," in *Electromagnetic Methods in Applied Geophysics*, vol. 2. Tulsa, OK, USA: Society of Exploration Geophysicists, 1991, pp. 521–640.
[7] L. Ma and M. Soleimani, "Magnetic induction tomography methods and applications: A review," *Meas. Sci. Technol.*, vol. 28, no. 7, Jul. 2017, Art. no. 072001.
[8] J. Jeon, W. Chung, and H. Son, "Magnetic induction tomography using magnetic dipole and lumped parameter model," *IEEE Access*, vol. 7, pp. 70287–70295, 2019.
[9] M. S. B. Mansor, Z. Zakaria, I. Balkhis, R. A. Rahim, M. F. A. Sahib, Y. M. Yunos, S. Sahlan, S. Bunyamin, K. H. Abas, M. H. I. Ishak, and K. A. Danapalasingam, "Magnetic induction tomography: A brief review," *J. Teknologi*, vol. 73, no. 3, pp. 91–95, Feb. 2015.
[10] L. Marmugi and F. Renzoni, "Optical magnetic induction tomography of the heart," *Sci. Rep.*, vol. 6, no. 1, Jul. 2016, Art. no. 23962.
[11] R. Liu, Y. Li, F. Fu, F. You, X. Shi, and X. Dong, "Time-difference imaging of magnetic induction tomography in a three-layer brain physical phantom," *Meas. Sci. Technol.*, vol. 25, no. 6, Jun. 2014, Art. no. 065402.
[12] R. Merwa, K. Hollaus, P. Brunner, and H. Scharfetter, "Solution of the inverse problem of magnetic induction tomography (MIT)," *Physiol. Meas.*, vol. 26, no. 2, pp. S241–S250, Apr. 2005.
[13] H.-Y. Wei and M. Soleimani, "Three-dimensional magnetic induction tomography imaging using a matrix free Krylov subspace inversion algorithm," *Prog. Electromagn. Res.*, vol. 122, pp. 29–45, Jan. 2012.
[14] L. Hasselgren and J. Luomi, "Geometrical aspects of magnetic shielding at extremely low frequencies," *IEEE Trans. Electromagn. Compat.*, vol. 37, no. 3, pp. 409–420, Aug. 1995.
[15] R. B. Schulz, V. C. Plantz, and D. R. Brush, "Shielding theory and practice," *IEEE Trans. Electromagn. Compat.*, vol. EMC-30, no. 3, pp. 187–201, Aug. 1988.
[16] D. A. Hill and J. R. Wait, "The electromagnetic response of a buried sphere for buried-dipole excitation," *Radio Sci.*, vol. 8, nos. 8–9, pp. 813–818, Aug. 1973.
[17] D. Miller and J. Bridges, "Review of circuit approach to calculate shielding effectiveness," *IEEE Trans. Electromagn. Compat.*, vol. EMC-10, no. 1, pp. 52–62, Mar. 1968.
[18] J. R. Wait, "Electromagnetic induction in a small conducting sphere above a resistive half space," *Radio Sci.*, vol. 3, no. 10, pp. 1030–1034, Oct. 1968.
[19] *EM Software and Systems, FEKO Suite 7.0*. Accessed: 2014. [Online]. Available: http://www.feko.info
[20] M. B. Cohen, U. S. Inan, and E. W. Paschal, "Sensitive broadband ELF/VLF radio reception with the AWESOME instrument," *IEEE Trans. Geosci. Remote Sens.*, vol. 48, no. 1, pp. 3–17, Jan. 2010.
[21] V. H. Harid, H. Y. Kim, M. Golkowski, S. D. Gedney, M. B. Cohen, S. K. Patch, R. A. L. Rorrer, C. M. Renick, J. Bittle, and N. M. Opalinski, "Magnetic field penetration into a metal enclosure using an ELF/VLF loop antenna," *IEEE Trans. Electromagn. Compat.*, early access, Dec. 18, 2019, doi: 10.1109/TEMC.2019.2952560.
[22] I. J. Won, D. A. Keiswetter, and T. H. Bell, "Electromagnetic induction spectroscopy for clearing landmines," *IEEE Trans. Geosci. Remote Sens.*, vol. 39, no. 4, pp. 703–709, Apr. 2001.
[23] M. Soleimani, "Super-sensing through industrial process tomography," *Philos. Trans. Roy. Soc. A, Math., Phys. Eng. Sci.*, vol. 374, no. 2070, Jun. 2016, Art. no. 20150445.

**HO Y. KIM** (Member, IEEE) received the Ph.D. degree in electronic and electrical engineering from the Pohang University of Science and Technology, Pohang, South Korea, in 2015.

From 2015 to 2016, he was a Postdoctoral Fellow with Pusan National University, Pusan, South Korea. Since 2016, he has been working as a Postdoctoral Fellow with the University of Colorado at Denver, Denver, CO, USA. His research interests include numerical modeling of low-temperature plasmas, electromagnetics, nonlinear wave-particle interactions in the earth's radiation belts, high-speed plasma science using hybrid-PIC, and PIC simulation.

**VIJAY HARID** (Member, IEEE) received the B.S. degree in electrical and computer engineering from the University of California at Santa Barbara, Santa Barbara, CA, USA, in 2009, and the M.S. and Ph.D. degrees in electrical engineering from Stanford University, Stanford, CA, USA, in 2012 and 2015, respectively. From 2015 to 2017, he was a Research Scientist with the Applied Physics Laboratory, Johns Hopkins University, where he focused on near-field magnetic imaging, ELF/VLF subionospheric communications, computational electromagnetics, and signals analysis. Since 2017, he has been an Assistant Professor with the Department of Electrical Engineering, University of Colorado at Denver. His current research interests include magnetospheric wave-particle interactions, ELF/VLF imaging and remote sensing, computational neuroscience, and computational plasma physics. He is a member of the American Geophysical Union, International Union for Radio Science.

**ALEXANDER MROZ** received the B.S. degree in electrical engineering from the University of Colorado at Denver, Denver, CO, USA, in 2019. He is currently pursuing the M.S. degree in electrical engineering with a focus in electromagnetics. In 2018, he joined the EM Research Group, University of Colorado. His research interests include ELF/VLF remote sensing, near-field imaging, and VLF communication hardware design.

**JOSHUA WEWERKA** is currently pursuing the B.S. degree in electrical engineering with the University of Colorado at Denver. He will also be working on his M.S. in Electrical Engineering expected spring 2020. He is a member of the Electromagnetics and Plasma Physics Research Group, where he works on VLF Imaging experiments and VLF hardware maintenance. His research interests include VLF remote sensing and robotics.

**DALIBOR J. TODOROVSKI** received the B.S. degree in physics from the University of Central Florida, Orlando, FL, USA, in 2016, and the M.S. degree in electrical engineering from the University of Colorado at Denver, Denver, CO, USA, in 2019.

He currently works as an Electrical Engineer with the Applied Physics Laboratory, Johns Hopkins University, where he focuses on problems in remote sensing, magnetics, and signals analysis. His current research interests include electromagnetic imaging and remote sensing.

**MARK GOŁKOWSKI** (Member, IEEE) received the B.S. degree in electrical engineering from Cornell University, Ithaca, NY, USA, in 2002, and the M.S. and Ph.D. degrees in electrical engineering from Stanford University, Stanford, CA, USA, in 2004 and 2009, respectively. He was a Postdoctoral Research Fellow with the Space, Telecommunications, and Radio Science Laboratory, Department of Electrical Engineering, Stanford University, from 2009 to 2010. He is currently a Professor with the Department of Electrical Engineering, University of Colorado at Denver. He actively conducts research on electromagnetic waves in plasmas, ionospheric physics, near-Earth space physics, and biomedical applications of gas discharge plasmas. He is a member of the American Geophysical Union. He was a recipient of the National Science Foundation CAREER Award, in 2013. He is currently the Chair of Commission H (Waves in Plasmas) for the U.S. National Committee for the International Union for Radio Science. He was an Associate Editor for the journal *Earth, Moon, and Planets*.

**RONALD A. L. RORRER** (Member, IEEE) was born in Heidelberg, West Germany, in 1962. He received the B.S. and M.S. degrees and the Ph.D. degree in mechanical engineering from V. P. I. & S. U., in 1984, 1985, and 1991, respectively.

From 1985 to 1986, he was a Precision Mechanical Design Engineer with Martin Marietta, Orlando, FL, USA. From 1992 to 1997, he was an Advanced Materials Project Leader with the Gates Rubber Company, Denver, CO, USA. Since 1997, he has been a Professor of mechanical engineering with the University of Colorado at Denver, USA. His research interests include tribology, composite materials, and alternative power systems.

**MORRIS B. COHEN** (Senior Member, IEEE) received the B.S. and Ph.D. degrees in electrical engineering from Stanford University, Stanford, CA, USA, in 2003 and 2010, respectively. He was a Research Associate with the Department of Electrical Engineering, Stanford University, until August 2013. From August 2012 to 2013, he was concurrently appointed as an AAAS Science and Technology Policy Fellow, serving at the National Science Foundation. In Fall 2013, he joined the School of Electrical Engineering, Georgia Tech, Atlanta, GA, USA, as an Assistant Professor, where he has been an Associate Professor with tenure, since August 2018. He has authored or coauthored 70 journal articles. His research interests include low-frequency radio wave generation, propagation, detection, and data science. He is currently the President-Elect of the Atmospheric and Space Electricity Section, American Geophysical Union. He is a 2014 winner of the Santimay Basu Prize by the International Union of Radio Science, in 2014, given once per three years to an under-35 Scientist. He also won the 2015 ONR Young Investigator Award, the 2017 NSF CAREER Award, and the 2018 Georgia Tech Junior Faculty Teaching Excellence Award.

**NATHAN M. OPALINSKI** received the B.S. degree in electrical engineering from Bucknell University, Lewisburg, PA, USA, in 2015, and the M.S. degree in electrical and computer engineering from the Georgia Institute of Technology, Atlanta, GA, USA, in 2017, where he is currently pursuing the Ph.D. degree in electrical and computer engineering with a focus in electromagnetics. In 2015, he was with the Low-Frequency Radio Group, Georgia Institute of Technology. His research interests include ELF/VLF remote sensing, electrically small antenna design, and machine learning. He was awarded the President's Fellowship from Georgia Tech.